DEVELOPMENT OF MONOLITHIC CERAMICS AND HIGH-TEMPERATURE COATINGS

Kennametal's Hot-Section Materials Development

Russell Yeckley, J. R. Hellmann, D. J. Green, E. C. Dickey, J. Adair, and Kevin Fox
Kennametal Inc.
1600 Technology Way, P.O. Box 231, Latrobe, PA 156-0231
Phone: (724) 539-4822, E-mail: Russ.yeckley@kennametal.com

Objective

Determine potential of an existing structural sialon that is being manufactured for other applications that, commensurate with the requirements of advanced microturbines shows potential for strength, environmental stability, and manufacturability for complex shapes.

Highlights

The sialon compositions selected for screening are centered on Kennametal's Ky1540 product. The sialons selected have the desired variation in composition and grain boundary structure to study effect on mechanical behavior and oxidation resistance. Mechanical testing should be complete this quarter.

Technical Progress

Kennametal's silicon nitride products have relatively simple geometries. Forming processes at Kennametal are primarily dry pressing. Other forming methods will be needed for microturbine components. Controlling AlN hydrolysis must be solved before water based processing could be used with the sialon materials. Penn State has a project within this program to develop a surfactant that will prevent AlN hydrolsis. The surfactant system will be transitioned to Kennametal and used to enable fabrication of near net shape tensile rods.

Current Progress

The four powders were characterized before experimentation began. The powder samples were viewed in a Hitachi S-3000H. BET Surface area measurements were performed on the Micromeritics Gemini. The results are listed in Table 1. X-ray diffraction patterns for each powder were obtained on the Scintag Pad V.

Table 1. BET surface area measurements

Sample ID	BET Surface Area (m2/g)
Alumina	9.3069
AlN	1.1040
Si3N4	2.8503
Yb2O3	3.7146

Initial zeta potential measurements have been completed on the Si_3N_4 powder and the AlN powder. The PMC has two methods to measure zeta potential. The Brookhaven ZetaPALS and the Dispersion Technologies 1200.

The Brookhaven ZetaPALS measures zeta potential using electrophoretic light scattering. An alternating electric field is applied to the particle suspension. As the particles move in the field the laser light is scattered. The scattered beam is measured by the detector and the zeta potential is calculated. The particle size range is 3 nm to 30 microns. A dilute suspension must be used on this instrument since the suspension has to be transparent and the particles must be stable in the suspension.

The DT 1200 combines acoustic and electroacoustic spectroscopy techniques. The acoustic spectroscopy measures the attenuation and sound speed of the ultrasonic pulses as they pass through the material. These measurements are made at various frequencies and the particle size distribution can be determined from the resulting data. The electroacoustic spectroscopy measures the interaction of electric and acoustic fields. The acoustic signal at a constant frequency is applied to the particle suspension causing the particles to vibrate. As the particles vibrate the associated double layers surrounding the charged particle vibrate. This displacement produces an electric field. The electric signal is called the Colloid Vibration Potential (CVP). The CVP induces a current in the dispersing medium, which is measured by the Colloidal Vibration Current (CVI). The zeta potential is calculated from the CVI. The acoustophoresis measures zeta potential for ceramic slurries with a minimum volume of one percent. It cannot measure particle sizes greater than 10 microns due to excessive scattering losses.

The zeta potential of the Si_3N_4 powder was measured using the DT1200 but the AlN powder run was unsuccessful in the DT1200 due to the larger particle size of the AlN powder. The zeta potential values for the AlN particles were measured using the ZetaPALS.

A 2.5 volume percent aqueous solution of the Si_3N_4 powder was prepared. A 1 M Nitric and and 1 M Tetraethyl ammonium hydroxide (TEAOH) solution were used to adjust the pH. The initial pH of the solution was pH 7. The pH versus zeta potential was measured from pH 7 to pH 10. And, a downward sweep from pH 10 to pH 5 was measured in order to cover the complete range from pH 5 to 10. The solution pH versus zeta potential curve for the two sweeps is shown in Figure 1.

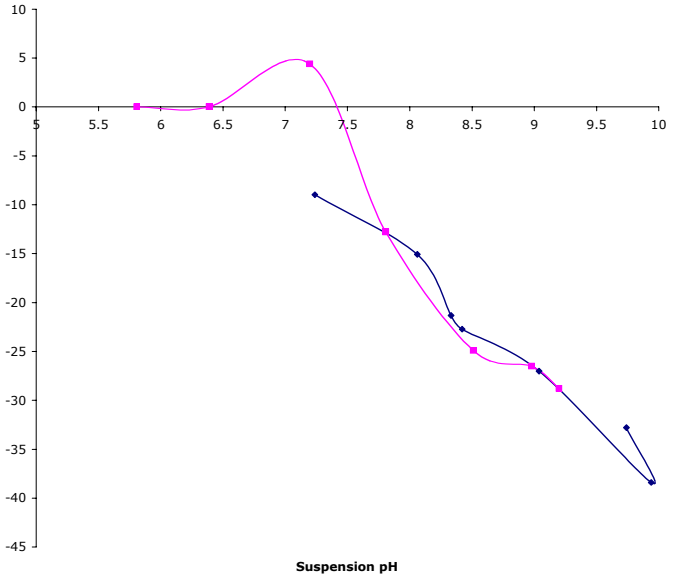

Figure 1. Zeta potential curve of Si3N4 in an aqueous suspension.

Figure 2 shows the solution pH versus zeta potential for the AlN powder with 0.5 M succinic acid and varying amounts of polyethylenimine (PEI) after one hour of equilibration. The amount of succinic acid used was 0.5 w/w based on the amount of AlN, which was determined in previous work done by Tarah Percora[1]. The PEI was varied from 0.1 to 3 w/w based on the amount of AlN in the suspension. In these experiments a 0.1 weight percent suspension was prepared for eight samples from pH 5 to pH 8. The pH of the suspension was varied using 1 M Nitric and 1 M TEAOH. The samples were shaken for one hour and then the zeta potential was measured on the ZetaPALS. After the measurement the samples were shaken for an additional 24 hours and another zeta potential measurement was made (Figure 3). As can be seen from the zeta potential graphs increasing the amount of PEI increased zeta potential of the particles and the pH increased with time.

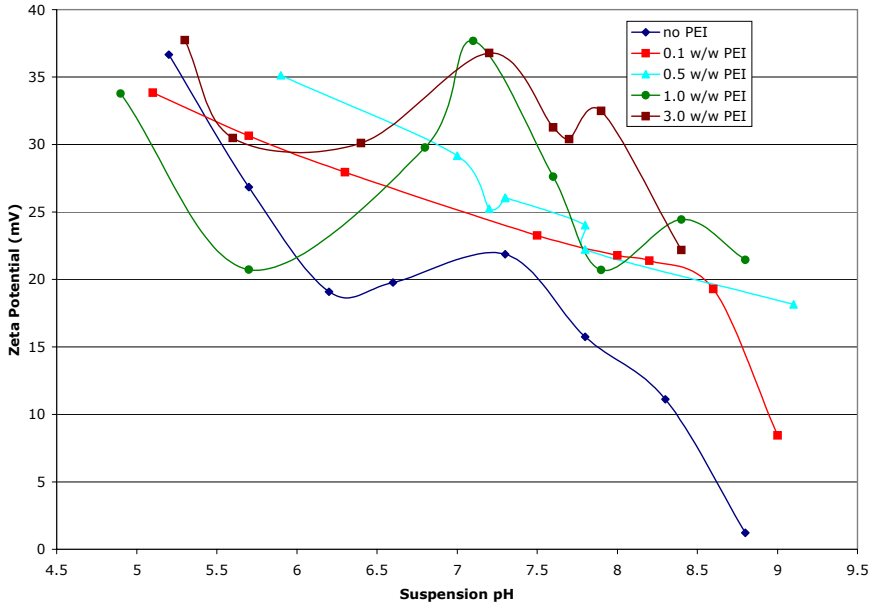

Figure 2. Zeta potential curve of AlN with varying amounts of PEI after 1 hour.

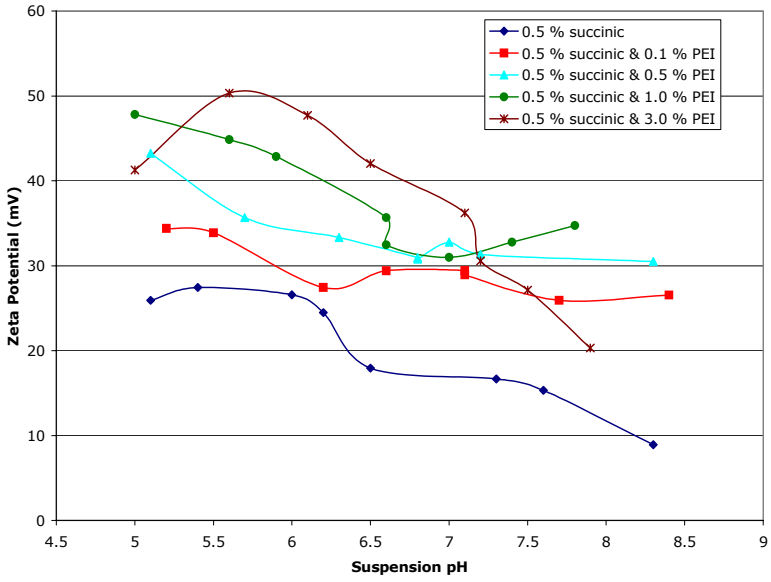

Figure 3. Zeta potential curve of AlN with varying amounts of PEI after 24 hours.

Reference

1. Tarah Pecora, James Adair, Michael Mandanas, *Surface Passivation and Dispersion of Aluminum Nitride for Aqueous Processing*, 1999.

Status of Milestones

Mechanical Testing of first sialon sample set is underway and should be complete this quarter.

Problems Encountered

Flexure machining delayed this milestone and the project. The use of biaxial testing to screen the sialons has been discussed as an approach to improve progress on sialon mechanical assessment.

Saint-Gobain Hot-Section Materials Development

R. H. Licht, Vimal K. Pujari, William T. Collins, Brian C. LaCourse, Ara M. Vartabedian
Saint-Gobain Ceramics & Plastics, Inc.
Goddard Road, Northboro, MA 01532
Phone: (508) 351-7815, E-mail: Robert.h.licht@saint-gobain.com

Objective

The goal of this Phase I program is to develop and optimize a high temperature silicon nitride based ceramic material and process suitable for microturbine hot-section component applications.

Highlights

The technical effort focused on the optimization of the as-processed (AP) surface properties of NT154. A proprietary HIP process mentioned in the previous report was utilized. The proprietary process continues to show expected improvements in AP strength. During this period, effort was directed toward its implementation in the production HIP.

In the area of complex shape forming, four fully-featured, radial rotors were fabricated based on an Ingersoll-Rand design. The rotors will be densified by the HIP process. Once densified, they will be used to establish process capability, dimension control, and material properties for the green forming method. In addition, the direct (starch) casting process was further optimized resulting in mechanical properties comparable to CIPed samples.

Microturbine OEM's were visited to explore the possibility of ceramic rotor testing.

Technical Progress

The technical effort involved a two-pronged approach:

1. Material development, and
2. Net Shape Forming Development (NSFD) involving the machining and Direct Casting (DC) approaches.

1. MATERIAL DEVELOPMENT:

   The improved AP properties reported in the previous report were achieved in a laboratory scale HIP. Initial experiments in a larger production HIP resulted in lower AP strengths for samples prepared using both the old and new processes. Despite the lower AP strengths, the new process still resulted in a strength improvement of up to

50%, which is comparable to that seen in the laboratory scale HIP. A new set of experiments has been planned to further investigate the AP properties obtained with the production HIP. Meanwhile, a parallel effort is underway to reproduce the previously reported excellent AP strengths in the laboratory scale HIP.

Mechanical testing of previously delivered test tiles is on-going at ORNL. The testing of the first set of delivered tiles is complete. The results are comparable to historical NT154 that had been optimized. Keiser Rig testing at ORNL is underway with baseline NT154 coupons.

2. NET SHAPE FORMING DEVELOPMENT (NSFD):

2.1 CNC Machining:

The optimized machining procedure described in previous reports was utilized to fabricate four radial turbine rotors according to an Ingersoll-Rand design (Figure 1). Dimensional control and surface finish parameters were established for the green rotor.

Based on the measurements, green rotors were fabricated with a ±0.004" (100 μm) tolerance and an overall average surface roughness of 28-36 μin (0.7-0.9 μm). The average surface roughness of the blades ranged from 25-32 μin (0.64-0.82 μm).

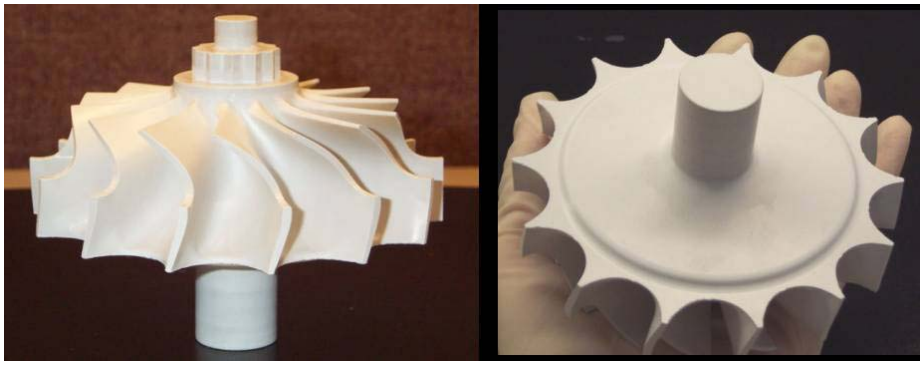

Figure 1: Green radial rotor.

These rotors will be densified by the HIP process and will be measured by CMM to ascertain the capability (dimensional control) of the forming process. Previous measurements on densified NT154 demonstration rotors suggested uniform dimensional shrinkage. This suggests that the green rotors mentioned above, after densification, should exhibit excellent dimensional control. In addition, the surface roughness of the dense rotors will be measured to determine the final value.

One or two of the densified rotors will be sent to ORNL for material property evaluation. These data will be compared against data obtained from tiles to determine the effect of the forming process. The data could also be used in any life prediction calculations.

2.2 Direct (Starch) Casting:

The optimized starch-containing slurry (OSS), with suitable binder content, solids loading, and surfactant, was used to fabricate 2" x 2" x 0.5" test tiles. Special precaution was taken during slurry preparation and its introduction into the flexible mold to minimize/eliminate any air bubble entrapment. This was verified by microfocus x-ray examination of the cast tiles. No visible defects were observed up to a 20X magnification.

In a parallel effort, the standard starch was replaced with a new type of starch (starch B). A cast tile, with the starch B containing slurry, experienced shrinkage during drying, which is negligible with the standard starch. This shrinkage is not desirable from a dimensional tolerance point of view. However, it did result in a higher green density and ultimately improved dense properties.

After binder burnout, the tiles were densified, by the HIP process, to near theoretical density. The surface finish and mechanical properties, measured on these tiles, were found to be comparable to those of CIPed tiles as shown in Table 1.

Table 1: Surface Roughness and Flexural Strength of Starch Cast Tiles

	CIPed NT154	**Standard Starch**	**Starch B**	**"OSS" (Standard Starch)**
Average Surface Roughness (μin)	40-50	96	46	92
Strength (MPa)	955	797	1002	791
Weibull Modulus	13	8	17	9

Status of Milestones

All milestones are on schedule. The third delivery of test tiles to ORNL, with improved AP properties, is still pending. A fully featured dense rotor is being fabricated for delivery to ORNL.

Industry Interaction

Vimal K. Pujari visited Capstone Corporation in California to meet with Matt Stewart and Frank Balas.

Ara Vartabedian, Bob Licht and Bill Donahue visited Wilson TurboPower to meet with David Wilson, Joern Kallmeyer, Rich McRay, and Bruce Anderson.

Problems Encountered

None

Publications/Presentations

None

Environmental Protection Systems for Ceramics in Microturbines and Industrial Gas Turbine Applications
Part A: Conversion Coatings

S. D. Nunn and R. A. Lowden
Metals and Ceramics Division
Oak Ridge National Laboratory
P.O. Box 2008, Oak Ridge, TN 37831-6068
Phone: (865) 576-1668, E-mail: nunnsd@ornl.gov

Objective

Monolithic silicon nitride ceramics are currently the primary ceramic material being used in combustion engine environments and are under consideration as hot-section structural materials for microturbines as well as other advanced combustion systems. Under oxidizing conditions, silicon nitride will typically form a surface oxidation (silicate) layer. In a combustion environment, this silicate layer can undergo rapid degradation because of the corrosive and erosive effects of high temperature, high pressure, and the presence of water vapor. This degradation can severely limit the useful life of the ceramic in this environment. Thus, the development of an environmental protection system for the ceramic has become an essential goal for enabling the long-term utilization of these materials in advanced combustion engine applications.

One approach that is being pursued to produce an environmental protection system for silicon nitride is the formation of a surface conversion layer using the pack cementation process. Pack cementation has been used for many years to develop an oxidation protection coating on nickel-based superalloys that are used for hot-section components in gas turbine engines. A reactive gas atmosphere is used to change the composition and microstructure of the metal alloy at the surface of the component so that it will form a protective oxide film under normal operating conditions. The same approach can be used to form a modified surface region on silicon nitride ceramic components. By selecting an appropriate reactive atmosphere for the pack cementation process, the surface region can be modified to form ceramic compounds that may provide enhanced corrosion and erosion resistance in the combustion engine environment.

Highlights

Visited both United Technologies Research Center and St. Gobain/Norton Northborough Research Center to discuss silicon nitride substrate materials and environmental barrier coating compositions and application methods.

Technical Progress

There was no technical progress during this reporting period. Funds to support technical work were exhausted at the end of the second quarter.

Status of Milestones

Examine surface conversion coatings for silicon-based ceramics containing zirconium, rare earth elements, and other compounds to enhance corrosion resistance. (Sept. 2003) Completed.

Industry Interactions

Visited United Technologies Research Center to present pack cementation coating results and to discuss environmental barrier coating processes and compositions.

Visited St. Gobain/Norton in Northborough, Mass. to review the restart of NT154 silicon nitride production and to discuss protective coatings for silicon nitride.

Problems Encountered

None

Publications and Presentations

A presentation on pack cementation coating efforts is being prepared for the EBC Workshop in November 2003.

Environmental Protection Systems for Ceramics in Microturbines and Industrial Gas Turbine Applications, Part B: Slurry Coatings and Surface Alloying

B. L. Armstrong, M. P. Brady, K. M. Cooley, J. A. Haynes, G. H. Kirby, and H. T. Lin
Metals and Ceramics Division
Oak Ridge National Laboratory
P. O. Box 2008, Oak Ridge, Tennessee 37831-6063
Phone: (865) 241-5862, E-mail: armstrongbl@ornl.gov

Objectives

Silicon-based monolithic ceramics are candidate hot-section structural materials for microturbines and other combustion systems. The performance of silica-forming ceramic materials in combustion environments is, however, severely limited by rapid environmental attack caused by the combination of high temperature, high pressure, and the presence of water vapor. Thus, the development of environmental protection systems has become essential for enabling the long-term utilization of these materials in advanced combustion applications.

Similar to thermal barrier coatings for nickel-based super alloys that utilize a specialized oxide surface layer and a metallic bond coat, successful environmental protection systems for ceramics and ceramic composites will likely utilize multiple layers and complex combinations of materials. Most recent efforts have focused on the selection and deposition of the oxide surface layer, and due to numerous factors, the majority of the candidates have been from the aluminosilicate family of oxide ceramics. Stable rare-earth silicate deposits have been found on component surfaces after recent engine and rig tests, indicating there may be other stable oxide compositions that have not been fully investigated. Thin coatings of selected silicate compositions will be deposited on test coupons using a variety of techniques. The specimens will then be exposed to simulated high-pressure combustion environments and materials that demonstrate good potential will be investigated further.

Highlights

Concentrated mullite and BSAS suspensions (= 0.45), which exhibit long-term stability, have been fabricated for use in a dip-coating process.

Technical Progress

Characterization of the BSAS and Mullite Slurries

Work continued on the optimization of mullite ($2SiO_2 + 3Al_2O_3$) and BSAS slurry compositions for a dip coating process. Zeta potential experiments were carried out in order to characterize the surface of the particles in aqueous suspension. Furthermore, experiments have been implemented to characterize the rheological properties, which can be tailored to control coating uniformity and thickness.

Zeta Potential Analysis

Zeta potential measurements were carried out as a function of pH for mullite and BSAS particles in dilute suspension (10^{-3} vol% solids) and the results are shown in Fig. 1. The isoelectric point (IEP) was observed at pH 3.8 and 3.2 for mullite and BSAS, respectively, which is near the IEP reported for pure SiO_2 (pH 2-3).[1] Interestingly, the measured IEP for the mullite system varies widely from reported values (pH 6-7). This result is particularly surprising because of its large content of Al_2O_3 (71.8 wt%), which has an IEP reported between pH 7 and 9.5. It is likely that the SiO_2 content, although small in comparison (28.2 wt%), governs the surface properties of this mullite powder. No literature values of the IEP were available for BSAS for comparison.

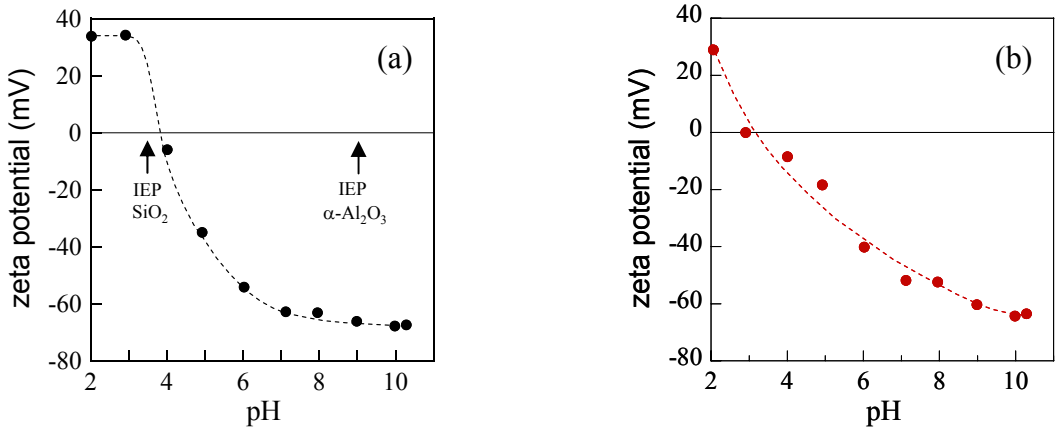

Fig. 1. Zeta potential as a function of pH for dilute (a) mullite and (b) BSAS suspensions (10^{-3} vol% solids). Note, the dashed lines merely guide the eye.

Development of Concentrated Mullite and BSAS Slurries

Previous work showed that the first mullite and BSAS slurries developed required further enhancement in stability. As these slurries aged, defects including thickness variation and uneven coverage were seen as a result of hydrolysis and agglomeration of the ceramic in the slurry. To solve these problems, a cationic polyelectrolyte (polyethylenimine, PEI), with a weight average molecular weight (M_w) of 10,000 g/mole and one amine group (NH) per monomer unit was implemented as a dispersant for these systems. The fraction of protonated amine groups, □, as a function of pH is shown in Fig. 2 (Note, □ = $[NH_2^+]/([NH] + [NH_2^+])$). This plot indicates that PEI is negligibly protonated at pH 11, but fully protonated at pH 5.5. Favorable conditions for adsorption of the PEI onto the ceramic particle surfaces exist at pH conditions between 4 and 8.8 where the PEI is highly positively charged (1 > □ > 0.5) and the ceramic powders are negatively charged. In turn, the adsorbed PEI layer, or adlayer, imparts electrosteric stabilization to the ceramic particles.[2, 3] Concentrated mullite and BSAS suspensions (45 vol% solids) suitable for a dip-coating process have been fabricated with the aid of the PEI dispersant.

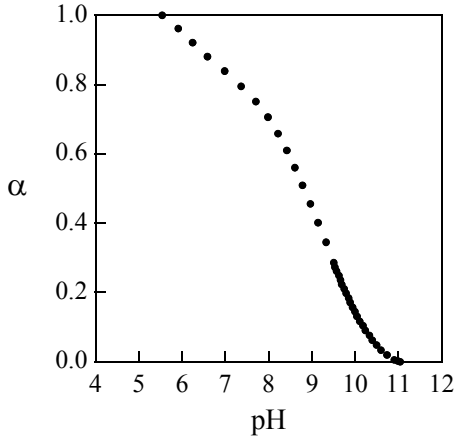

Fig. 2. Fraction of protonated amine groups, α, as a function of pH in dilute PEI solution (10^{-3} *M*). Note, $\alpha = [NH_2^+]/([NH] + [NH_2^+])$.

Rheological experiments are underway to measure the apparent viscosity (η_a), linear elastic shear modulus (G'), and yield stress (τ_Y) of concentrated mullite- and BSAS-PEI suspensions (45 vol% solids). Preliminary results are shown in Figs. 3 and 4 for the mullite and BSAS systems, respectively. The mullite suspensions were prepared at a constant pH of 4 and varying PEI weight fraction. Likewise, a BSAS suspension with 10 mg PEI/g BSAS was prepared. A constant pH of 4 could not be maintained as hydrolysis of the BSAS particles occurred below pH 6.5; therefore, a constant pH of 7 was maintained.

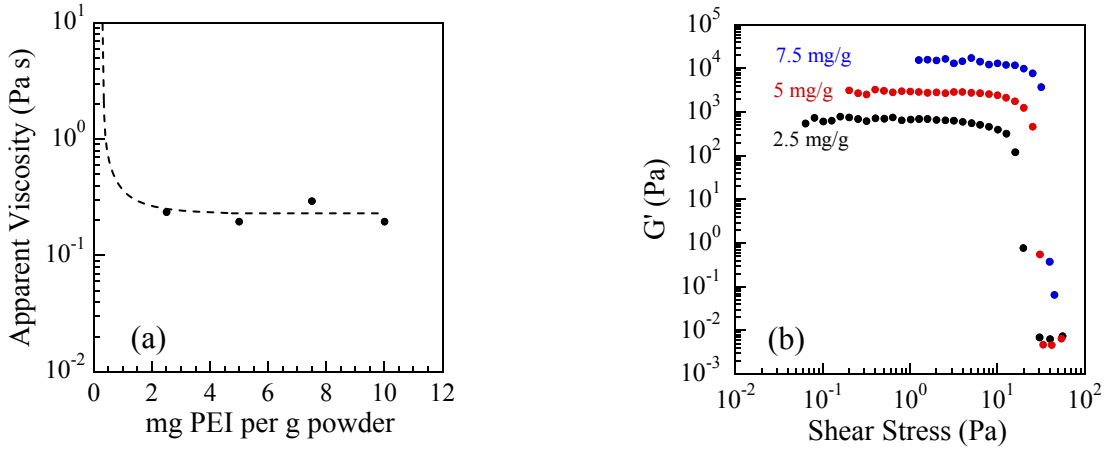

Fig. 3. The rheological behavior of concentrated mullite suspensions (45 vol% solids) at pH 4: (a) The apparent viscosity, measured at a constant shear stress of 200 Pa, is plotted as a function of PEI weight fraction (mg PEI/g mullite). Note, the dashed line merely guides the eye. (b) The elastic shear modulus, measured at an applied frequency of 1 Hz, is plotted as a function of oscillatory shear stress for suspensions of varying PEI weight fraction.

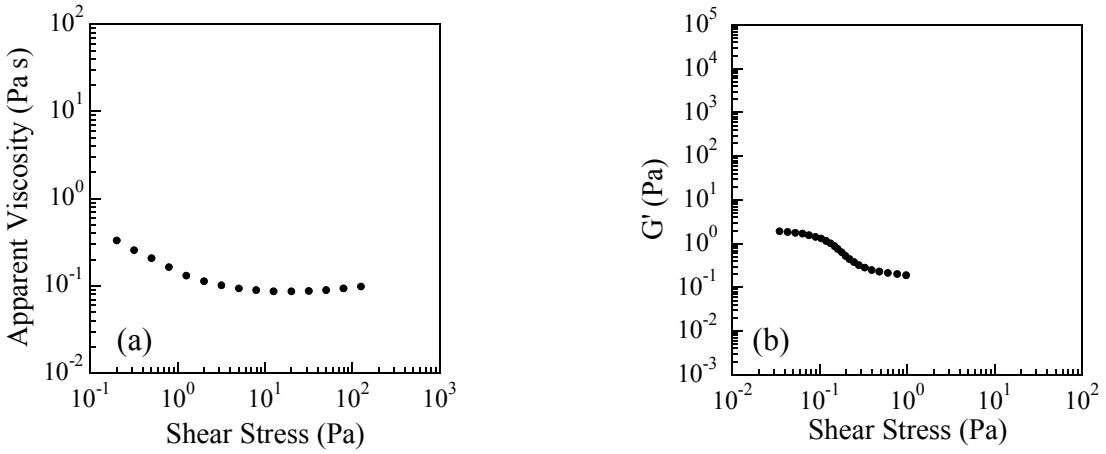

Fig. 4. The rheological behavior of concentrated BSAS suspensions (45 vol% solids) at pH 7: (a) The apparent viscosity is plotted as a function of applied shear stress for a suspension with 10 mg PEI/g BSAS. (b) The elastic shear modulus, measured at an applied frequency of 1 Hz, is plotted as a function of oscillatory shear stress for a suspension with 10 mg PEI/g BSAS.

For mullite and BSAS suspensions in the absence of PEI, the apparent viscosities were very high and beyond the measurement capability of the rheometer. For mullite suspensions with PEI additions ranging from 2.5 to 10 mg per gram of mullite, shear thinning behavior and low apparent viscosities (~ 0.15 Pa s) at an applied shear stress of 200 Pa were observed (see Fig. 3(a)). In comparison, slightly shear-thinning flow behavior and an apparent viscosity of 0.15 Pa·s at 200 Pa shear stress was observed for the BSAS-PEI suspension in Fig. 4(a). These rheological properties suggest excellent suspension flow behavior for mixing, pouring, and dipping operations.

These mullite- and BSAS-PEI suspensions exhibit gel-like behavior, as shown by the elastic properties in Figs. 3(b) and 4(b), respectively. Mullite suspensions with 2.5 mg, 5 mg, and 7.5 mg of PEI per gram of mullite had linear elastic modulus values of 687 Pa, 2,860 Pa, and 14,500 Pa, respectively, and yield stress values of 15 Pa, 24.5 Pa, and 30 Pa, respectively. The gel strength was weaker for the BSAS-PEI suspension, which had a linear elastic modulus and yield stress value of 1.5 Pa and 0.1 Pa, respectively. Optimizing the gel strength for the dip-coating process an ongoing process, and future work will explore how coating uniformity and thickness may vary with the linear elastic modulus and yield stress, which can be tailored by adjusting the PEI concentration, pH, and ionic strength (salt content).

Development of a Sacrificial Coating

No work to report this quarter.

Status of Milestones

Evaluate the protective capacity of new silicate coatings on Si_3N_4 in simulated combustion environment. (Completed June 2002)

Industry Interactions

Discussions with UTRC have continued. This project has also collaborated with an ARTD Fossil Energy project on Corrosion Resistant Coatings.

Problems Encountered

None

Publications

None

References

1. Reed, J.S., *Principles of Ceramic Processing*. 2nd ed. 1995, New York, NY: John Wiley & Sons. 658.

2. Cesarano, J., "Stability of Aqueous a-Al_2O_3 Suspensions with Poly(methacrylic acid) Polyelectrolyte," *J. Am. Ceram. Soc.*, **71** (4) 250-55 (1988).

3. Cesarano, J., "Processing of Highly Concentrated Aqueous a-Alumina Suspensions Stabilized with Polyelectrolytes," *J. Am. Ceram. Soc.*, **71** (12) 1062-67 (1988).

Failure Mechanisms in Coatings

J. P. Singh, K. Sharma, and P. S. Shankar
Energy Technology Division
Argonne National Laboratory
Argonne, IL 60439
Phone: (630) 252-5123, E-mail: jpsingh@anl.gov

Objective

The purpose of this research is to identify failure mode(s), understand and evaluate failure mechanisms, and to develop appropriate test methods and protocols to characterize the integrity and predict failure of environmental and thermal barrier coatings for advanced turbine applications.

Highlights

Four-point flexure strength of AS800 silicon nitride (Si_3N_4) substrates coated with an environmental barrier coating (EBC) of pure tantalum oxide (Ta_2O_5) has been evaluated. The strength of the coated specimens was 432.1±82.4 MPa, as compared to 708.9±58 MPa for the uncoated Si_3N_4 specimens. Failure in these specimens was observed to initiate from the pores/voids at the substrate/coating interface.

Technical Progress

This quarter, effort was initiated on evaluating four-point flexure strength of AS800 Si_3N_4 substrates coated with Ta_2O_5 EBC. Specifically, three coated substrates (50 mm x 26 mm x 4 mm) were received from Northwestern University/Honeywell. The substrates were coated with Ta_2O_5 EBC using the small particle plasma spray process [1]. These substrates had received a 1250°C soak and were preheated to 450°C before spraying. Flexure bars of dimension 26 x 2 x 1.5 mm were machined (using a diamond saw) from one of the coated substrates (with pure Ta_2O_5 EBC). The other two coated substrates had different additions to the Ta_2O_5 EBC. The edges of the flexure bars were beveled (1 μm diamond) before testing to minimize edge failure. Four bars were tested according to ASTM C1161-94 specification (configuration-A) with the coating surface loaded in tension. In addition, four uncoated AS800 Si_3N_4 flexure bars of the above-noted dimensions were also machined from the same substrate and tested under identical conditions as that of the coated specimens.

Figure 1 shows the measured four-point flexure strength of uncoated and Ta_2O_5 coated AS800 Si_3N_4 specimens. The flexure strength of the Ta_2O_5 coated specimens was 432.1±82.4 MPa, which is significantly lower than that of the uncoated AS800 Si_3N_4 specimens (708.9±58 MPa). It is to be noted that the strength of the coated specimens was calculated by taking thickness of the Si_3N_4 substrate as the total thickness of the specimen. The observed strength degradation

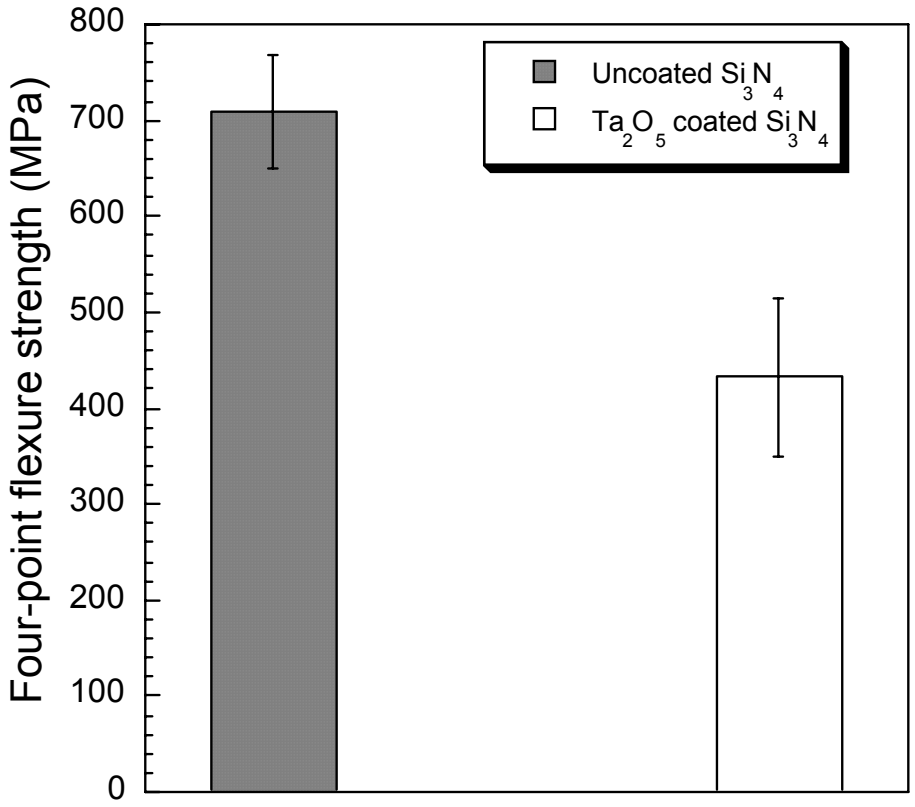

Figure 1. Four-point flexure strength of the uncoated and Ta_2O_5 - coated AS800 Si_3N_4 specimens. The error bars represent standard deviation around the mean strength value.

may be associated with residual stresses at the interface due to thermal expansion mismatch between the Si_3N_4 substrate and Ta_2O_5 EBC.

Fractographic evaluation was performed on all the four-point flexure bars and critical flaws were identified by standard fractographic techniques. All bars failed within the inner loading span (away from the loading pins). One of the bars failed from the edge flaw, and was excluded from the average strength calculations. The remaining bars failed from the microstructural defects such as shown in Figure 2. The figure shows the fracture markings (at low magnification) of a Ta_2O_5 coated AS800 Si_3N_4 specimen and the critical flaw (at high magnification) at the failure origin. The critical flaw in this case is associated with the presence of voids at the substrate/coating interface. Currently, microindentation testing and detailed stress analysis at the interface are in progress to understand the observed strength degradation in the Ta_2O_5 coated Si_3N_4 specimens relative to the uncoated specimens. Also, mechanical and microstructural evaluations of the coupons with different EBC compositions are in progress.

Reference

1. Monica Moldovan, C. M. Weyant, D. Lynn Johnson and K. T. Faber, "Tantalum Oxide Coatings as Candidate Environmental Barriers," J. Thermal Spray Technology (in press).

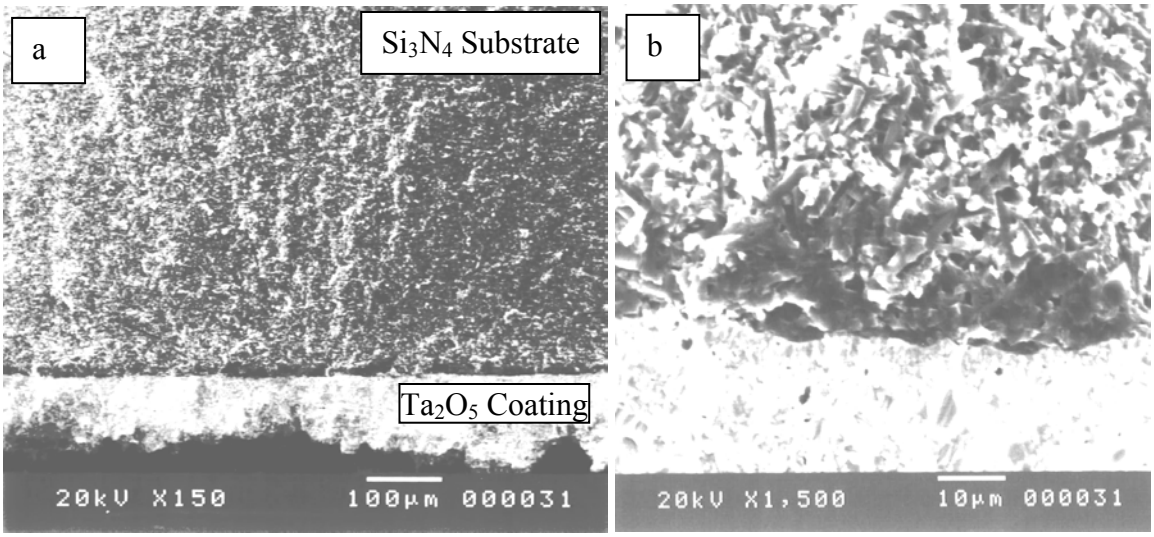

Figure 2. Micrographs of a Ta_2O_5 - coated AS800 Si_3N_4 specimen showing (a) the fracture markings at the failure origin (at low magnification), and (b) the critical flaw (interfacial voids) at the failure origin.

Status of Milestones

Perform mechanical strength testing (four-point) and fractographic evaluations of the first set of pure Ta_2O_5 coated AS800 Si_3N_4 and BSAS Coated SN282 specimens, September 2003. On schedule.

Industry Interactions

Discussion on the results of mechanical and microstructural evaluation of Ta_2O_5 coated AS800 Si_3N_4 specimens were continued with Northwestern University/Honeywell.

Problems Encountered

None

Publication

J. P. Singh will present a talk entitled, " Mechanical and Fractographic Evaluations of Si_3N_4 Substrates and EBCs", at the 'Environmental Barrier Coatings for Microturbine and Industrial Gas Turbine Ceramics' workshop to be held in Nashville, TN on November 18-19, 2003.

Recuperator Alloys – Composition Optimization for Corrosion Resistance

B. A. Pint
Metals and Ceramics Division
Oak Ridge National Laboratory
Oak Ridge, TN 37831-6156
Phone: (865) 576-2897, E-mail: pintba@ornl.gov

Objective

In order to provide a clear, fundamental understanding of alloy composition effects on corrosion resistance of stainless steel components used in recuperators, the oxidation behavior of model alloys is being studied. The first phase of this study narrowed the range of Cr and Ni contents required to minimize the accelerated corrosion attack caused by water vapor at 650°-800°C. Other factors that continue to be investigated include the effects of temperature, alloy grain size, phase composition and minor alloy additions. These composition and microstructure effects also will provide data for life-prediction models and may suggest a mechanistic explanation for the effect of water vapor on the oxidation of steels. This information will be used to select cost-effective alloys for higher temperature recuperators.

Highlights

The oxidation behavior of model austenitic alloys is being studied in order to better understand the role of minor alloy additions on the accelerated attack (AA) observed in exhaust gas at 650°C-700°C. Results from a series of alloys based on Fe-(16-20)Cr and (15-20)Ni illustrated that the leaner compositions Fe-16Cr-15Ni all were susceptible to AA in humid air at 650°C despite various additions of Mn, Si and/or La. When the Cr and/or Ni content was increased to 20% in the base alloy, additions of Mn and Si significantly improved resistance to AA. For a base alloy of Fe-20Cr-20Ni, single additions of Mn, Si and La did not prevent the onset of AA. However, when both Mn and Si were added, no AA has been observed after more than 5,000h of testing at 650°C in humid air.

Technical Progress

Experimental Procedure

As outlined in previous reports, model alloys were vacuum induction melted and cast in a water-chilled copper mold, followed by hot forging and rolling to 2.5mm. The sheets were then cold rolled to 1.25mm and annealed under Ar + 4%H_2 for 2 min at 1000°C. Sheet specimens (12mm x 17mm x 1.2mm) were polished to 600 grit SiC finish. Chemical compositions were measured by combustion and plasma analysis after casting, Table I. The oxidation tests were done in air + 10 vol.% water vapor with 100h cycles at 650°. After oxidation, selected specimens were Cu-plated, sectioned and polished to examine the oxide scale.

Results of oxidation testing

Previous work on model ferritic alloys had shown that Mn and Si were two of the most beneficial minor alloy additions for preventing AA and retaining a thin, protective surface oxide. (High mass gains after the onset of AA indicate the formation of a thick oxide, while large mass losses indicate

Table 1. Alloy chemical compositions (mass %) and average grain sizes (μm)

Material	Cr	Ni	Mn	Si	C	N	Nb	Ti	Mo	Other	aver. grain size
Fe-20Cr-20Ni	19.7	20.1	<	0.01	<	<	<	<	<		14μm
Fe-16Cr-15Ni	15.8	14.8	<	<	0.002	<	<	<	<		24
Fe-16Cr-15Ni+Mn	16.0	15.0	1.66	0.01	0.002	0.001	<	<	<		≈15
Fe-16Cr-15Ni+Si	16.2	14.7	<	0.17	<	0.001	<	<	<		
Fe-16Cr-15Ni+La	16.1	14.9	<	0.01	0.001	0.02	<	<	<	0.17 La	
Fe-16Cr-15Ni+MS	15.8	14.8	1.76	0.24	<	<	<	<	<		
Fe-16Cr-15Ni+MSL	17.0	14.1	1.74	0.24	0.002	0.001	<	<	<	0.17 La	
Fe-16Cr-20Ni+MS	15.8	19.7	1.72	0.24	0.003	0.001	<	<	<		
Fe-20Cr-15Ni+MS	19.8	14.9	1.70	0.24	0.001	0.007	<	<	<		
Fe-20Cr-20Ni+Mn	20.0	19.8	1.47	0.01	0.002	0.001	<	<	0.01		
Fe-20Cr-20Ni+Si	19.9	19.7	<	0.23	0.001	0.005	<	<	<		
Fe-20Cr-20Ni+La	20.3	19.7	<	<	0.001	0.001	<	<	<	0.10 La	
Fe-20Cr-20Ni+MS	19.8	19.8	1.69	0.25	<	0.003	<	<	<		
Fe-20Cr-20Ni+MSL	20.2	19.9	1.61	0.22	0.001	0.011	<	<	<	0.12 La	
Fe-20Cr-20Ni+etc.	20.9	20.8	3.8	0.24	0.08	0.18	0.25	<	0.31	0.3 Cu, 0.3Co	

< indicates below the detectability limit of <0.01% or <0.001% for interstitials

the spallation of the thick oxide.) In order to clarify the role of these additions in austenitic alloys, model alloys were made with various additions of Mn, Si and La, Table I. Figure 1a shows the 650°C performance of various alloys with a base composition of Fe-16Cr-15Ni. All of the additions showed

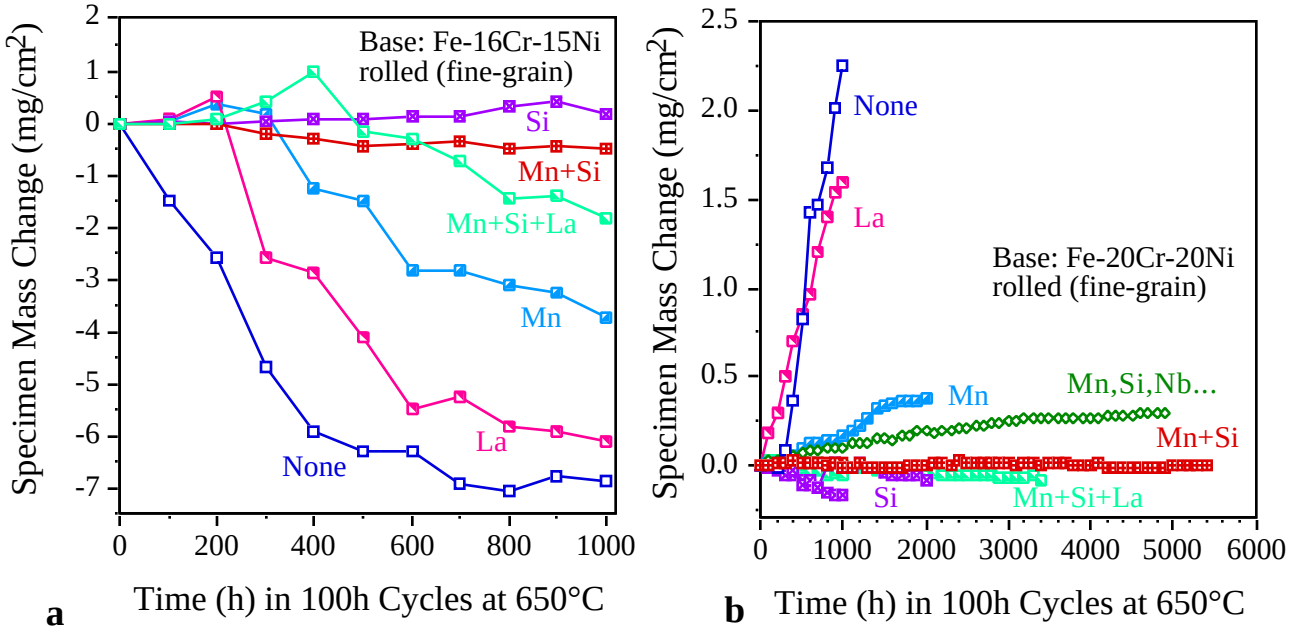

Figure 1. Specimen mass changes for model Fe-Cr-Ni alloys during 100h cycles at 650°C in air plus 10%H_2O, (a) alloys with a base composition of Fe-16Cr-15Ni and (b) alloys with a base composition of Fe-20Cr-20Ni. Note the change in the y-axis range between (a) and (b).

less mass loss than the base alloy without additions, but all of the modified alloys showed AA to some degree. Single additions of La or Mn showed the least benefit. Surprisingly, the addition of Si alone showed less mass change than the additions with Si in combination with Mn or Mn and La. In general, these results suggest that the base Fe-16Cr-15Ni alloy is too lean in Cr and Ni to be protective under these conditions. With a base composition of Fe-17Cr-11Ni, a similar inference can be drawn about type 347 stainless steel.

Figure 1b shows the performance of various modifications of a base Fe-20Cr-20Ni alloy at 650°C. Again, single additions of Mn or La did not show a significant beneficial effect. The onset of AA was slowed by the Mn addition but not prevented. Linear mass losses were observed for the alloy with only a Si addition. These small mass losses are attributed to evaporation of Cr from the scale. However, the edges of the specimen showed evidence of the onset of AA. The addition of both Mn and Si led to a low mass change past 5,000h thus demonstrating a synergistic benefit of adding both elements. Adding La in addition to Mn and Si has not shown any additional benefit at this stage of the testing, Figure 1b. The first attempt to develop a creep-resistant version of Fe-20Cr-20Ni contains additions of Mn, Si, Nb and several other elements, Table I. The oxidation behavior of this material also is shown in Figure 1b. The mass gain is higher than the model alloy with only Mn and Si additions but no AA has been observed after almost 5,000h. The higher mass gain is attributed to its higher Mn content which can lead to additional Mn-rich spinel formation.

Since the best long-term behavior was noted with additions of Mn and Si, additional model alloys were made with different Cr and Ni contents. Figure 2 shows the performance of several of these alloys at 650°C in humid air compared to the base model alloys without Mn and Si additions. In each case, the addition of Mn and Si improved the resistance to AA compared to the base alloy. However, as noted above, with Fe-16Cr-15Ni, the addition of Mn and Si reduced the mass loss compared to the

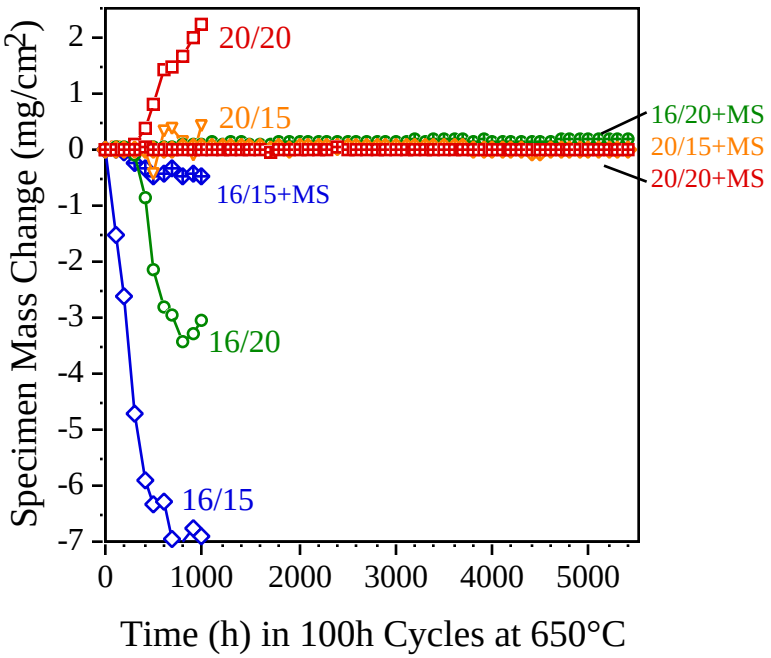

Figure 2. Specimen mass changes for model Fe-Cr-Ni alloys (specified by their Cr/Ni contents) during 100h cycles at 650°C in air plus 10%H_2O. Designations with "+MS" indicate Mn and Si additions.

base alloy but did not prevent AA. Figure 3a shows the scale cross-section after 1000h at 650°C on Fe-16Cr-15Ni+Mn,Si. The typical duplex scale was observed with an outer Fe-rich oxide and an inner mixed Fe, Cr, and Ni oxide. A similar oxide was observed on all of the model alloys without Mn and Si additions. For example, Figure 3b shows the scale formed on Fe-20Cr-20Ni after 1000h. Increasing either the Cr or Ni content to 20% and adding Mn and Si eliminated the onset of AA to over 5,000h, Figure 2. Cross-sections of Fe-16Cr-20Ni+Mn,Si and Fe-20Cr-15Ni+Mn,Si after 1,000h at 650°C are shown in Figures 3c and 3d, respectively. A few oxide nodules were observed on the former material but based on the low, long-term mass gain, the nodules did not continue to grow significantly. Only small nodules were observed on Fe-20Cr-15Ni+Mn,Si, Figure 3d. Increasing the Cr and Ni contents to 20% with the additions of Mn and Si resulted in very little mass change after a 5,000h exposure at 650°C and a uniform thin scale, Figure 3e. Because of its thin scale and low mass change, this alloy is considered the most promising composition for further development.

Some of the other model alloys also were sectioned and are shown in Figure 3. The mass losses noted for Fe-20Cr-20Ni+Si resulted in a thin scale after a 1000h exposure at 650°C, Figure 3f. The higher mass gain for Fe-20Cr-20Ni+Mn can be attributed to the large oxide nodules observed in Figure 3g.

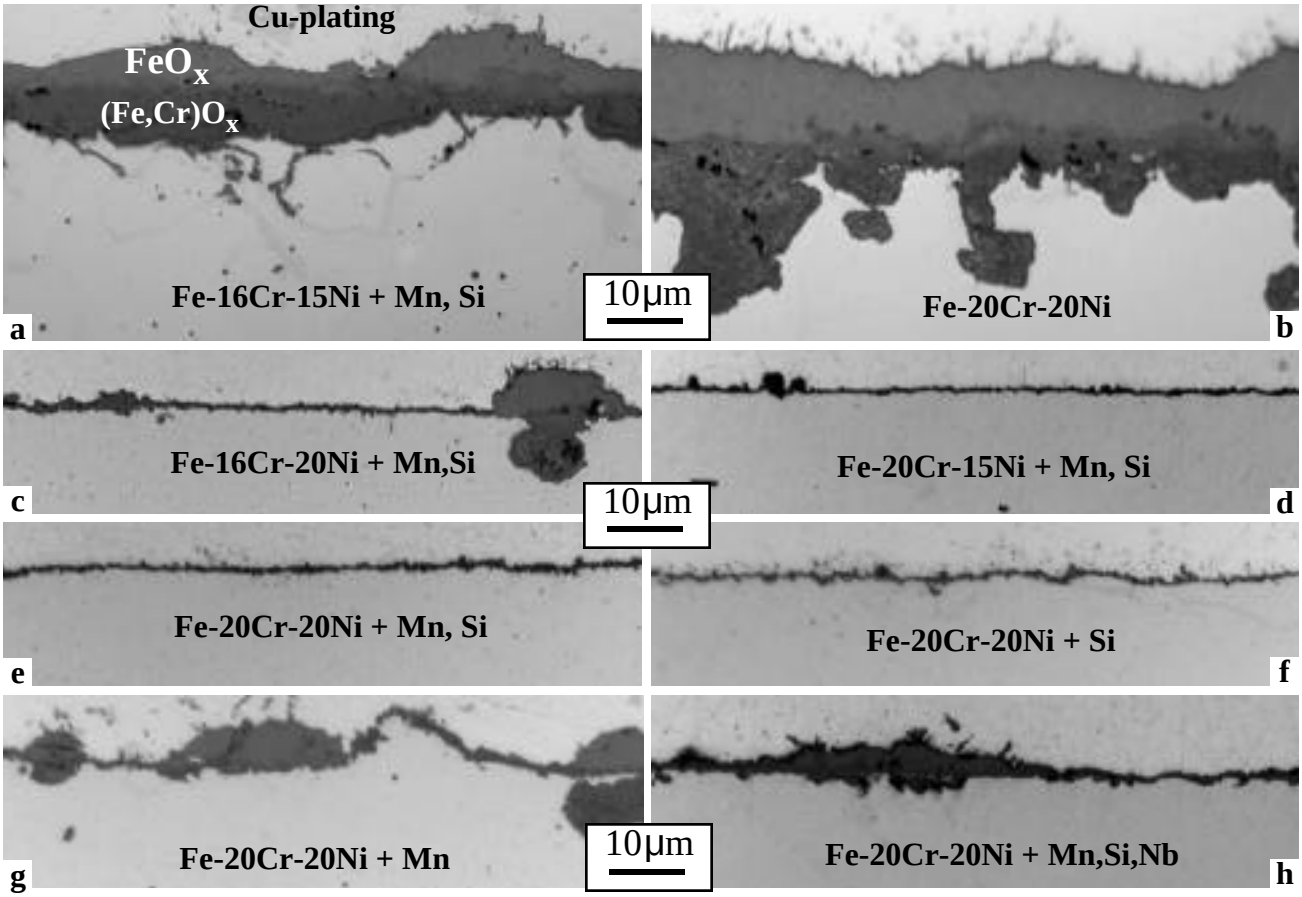

Figure 3. Light microscopy of polished cross-sections of model alloys oxidized for 1000h at 650°C in humid air (a) Fe-16Cr-15Ni+Mn,Si, (b) Fe-20Cr-20Ni, (c) Fe-16Cr-20Ni+Mn,Si, (d) Fe-20Cr-15Ni+Mn,Si, (e) Fe-20Cr-20Ni+Mn,Si, (f) Fe-20Cr-20Ni+Si, (g) Fe-20Cr-20Ni+Mn, and (h) Fe-20Cr-20Ni+Mn,Si,etc.

Finally, Figure 3h shows the thicker scale formed on the creep-resistant version of Fe-20Cr-20Ni, likely due to its higher level of alloy additions. Future development work will examine alloy additions that improve the alloy creep strength while minimizing the scale thickness.

Status of Milestones

Draft a report summarizing results on the use of minor alloy additions to improve corrosion performance in exhaust gas environments. (January 2003) Completed - NACE Paper #03-499.

Industry Interactions

Visited Ingersoll Rand in New Hampshire in July 2003 to discuss materials selection issues.

Provided oxidation data on alloy foils to Wendy Matthews at Capstone.

Problems Encountered

None.

Publications/Presentations

None.

POWER ELECTRONICS

Heat Exchange Concepts utilizing Porous Carbon Foam

B. E. Thompson and Anthony G. Straatman
The University of Western Ontario
Faculty of Engineering
London, Ontario, Canada N6G 4K1
Phone: (519) 850-2530, E-mail: Thompson@eng.uwo.ca

Objective

There is a need to produce engineering models for design of heat exchangers made from emerging porous carbon-foam materials. Knowledge and understanding of the effects of carbon foam on convective heat transfer is crucial to the development of appropriate engineering approximations for these design models. The overall objective is to explore new ideas for heat-exchanger configurations, especially for situations in which current technology is marginally cost effective. A thermo-economic model and a strategic design study are planned to provide new understanding for assessment in a stage-gate approach to further prototype development.

Highlights

A combination of engineering-design and computational activities have been initiated to obtain new understanding and knowledge about interstitial flow through carbon foam that affects the effective surface area for heat transfer and about the effects of roughness and pore size on flow over carbon foam. Preliminary results obtained on automotive radiators suggest heat transfer enhancement could be significant if the pores size, permeability and geometry of carbon-foam components were designed appropriately.

Technical Progress

Two phenomena appear likely to enhance convective heat transfer in flow over a porous carbon-foam surface: first, increased mixing in flow over the surface and, second, interstitial flow that increases the surface area on which convection transfers heat in an array of bubble pores.

An engineering model has been configured to predict performance of air-water radiators made from porous carbon foam. Its empirical constants have been quantified although from only one ORNL heat-exchanger experiment. Configuration of computational methods to predict convective heat transfer in flow over porous carbon foam has been initiated and, after development is complete, will be used to provide insight into the two aforementioned phenomena that are expected to strongly influence these empirical values. In addition, additional experiments needed to make these constants more generally applicable have been designed and are under discussion with ORNL and Western technical personnel.

Status of Milestones

The next milestone is a model of carbon foam that will provide insights into the importance of pore diameter and permeability on available surface area and potential for enhanced mixing. The development of this model will move the team closer to its goal of designing a carbon-foam replacement for a commercial recuperator in a microturbine, which has been chosen for detailed study.

Industry Interactions

Unifin has helped Western to obtain better understanding of heat-exchanger performance and selection issues for microturbine applications.

Problems Encountered

Experimental results from which the values of empirical constants for porous-carbon foam can be obtained, are needed. The quantity of existing data is insufficient for the range of problems of practical interest in microturbines. A test program to obtain the necessary data for a practical range of porosity, pore size and fin geometries is needed.

Publications/Presentations

None

MATERIALS FOR ADVANCED RECIPROCATING ENGINES

Advanced Materials for Exhaust Components of Reciprocating Engines

P. J. Maziasz and N.D. Evans
Metals and Ceramics Division
Oak Ridge National Laboratory
P.O. Box 2008, Oak Ridge, TN 37831-6115
Phone: (865) 574-5082, E-mail: maziaszpj@ornl.gov

Objective

This program has addressed the general high-temperature and performance limitations of various critical exhaust components (exhaust valve, exhaust manifold, turbocharger housing) for advanced natural gas reciprocating engine systems (ARES). It is currently focused on the Ni-based superalloy exhaust valves that advanced ARES engines are using, and are pushing to higher temperatures. This program began by assessing the performance of current valves and coatings systems, and is moving into a development phase to modify the alloys and processing or the coatings, in order to achieve reliable performance at higher temperatures.

Highlights

ORNL has completed detailed microcharacterization of Ni-based superalloy exhaust valves provided by Waukesha Engine Division, Dresser Industries, Inc. and their component supplier, TRW Automotive Division, TRW, Inc. Significant effects of aging can be seen in the microstructure during service relative to fresh valves. Valves exposed to higher temperatures have been requested from Waukesha. The new focus of this project is to compare the properties of some alternate commercial or developmental superalloys for valves, consider processing or alloying adjustments, and to consider coatings that can push reliable performance to higher temperatures.

Technical Progress

Nickel-based superalloys like Nimonic 80A, 90, Pyromet 31 and Waspaloy are used to make exhaust valves for a variety of advanced diesel and ARES engines. These valves are complex systems, with weld-overlays on the valve seat, and coatings on the combustion face. The fillet region of the exhaust valve can see temperatures approaching 700^{o}C, and advanced ARES engines will likely have even higher temperatures. High-temperature engine exposure changes the base-metal microstructure and mechanical properties as well as the structure at the coating and base-metal interface.

Microcharacterization of exhaust valves of Pyromet 31V (Ni-22Cr-15Fe alloy with Ti and Al for γ' precipitation hardening) were provided by Waukesha Engine Division, Dresser Industries, Inc. and their component supplier, TRW Automotive Division, TRW, Inc., and microcharacterization of the valve seat with an Co-Cr-W alloy weld overlay of the fresh valve is shown in Fig. 1.

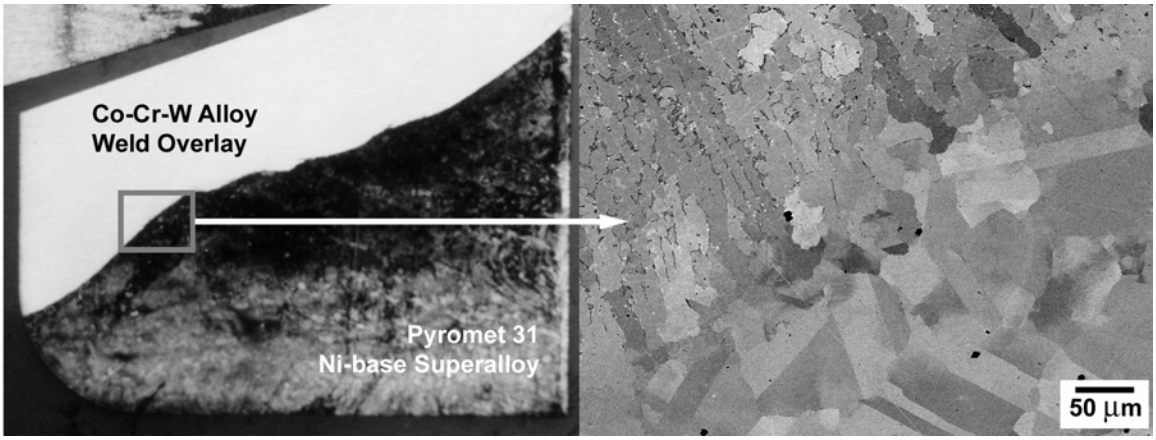

Figure 1 – Microcharacterization of the valve seat region of a fresh valve, showing the Co-Cr-W weld overlay and the basemetal underneath.

Aging during engine service produces significant changes in microstructure, including grain structure and the various precipitate phases. Microcompositional analysis to identify the various phases in the fresh and engine exposed valves has been complete and will be reported next quarter. Transmission electron microscopy to observe intragranular precipitation, and several hardness profiles to determine hardening or softening during service will complete this effort.

Last quarter, valves with higher temperature exposure in advanced engines were requested. Caterpillar has also been contacted about interest in exhaust valves with higher temperature capability. A range of commercial valve alloys can be identified that may have higher temperature capability, particularly with minor compositional changes, and forged rod stock of these alloys can be used for mechanical testing. One example is the alloy 718 Plus recently developed by Allvac to have improved performance compared to Wasploy without low ductility and higher cost of this Ni-Co superalloy. Another example is alloy 740, developed by Special Metals for fossil boiler tubing applications, but which can also be considered for exhaust valves. Advanced coatings are another way to economically enhance oxidation and wear resistance at higher temperatures relative to conventional valves.

Status of Milestones

FY 2003 – Complete characterization of TRW/Waukesha Ni-based superalloy valves to define changes during service and potential performance limitations. Identify metallurgical/weld-overlay or coating avenues for improved performance and reliability (May 2003) – completed.

Industry Interactions

Interactions with Waukesha Engine Dresser, Inc. (Joe Derra, Manager of Materials and Analysis) and TRW Engine Components (Victor Levin, Manager-Materials Engineering) about examining current exhaust valves with more severe engine exposure, and about developing valves with improved performance continued this quarter. Contact has been made with Caterpillar concerning their interest in exhaust valve, and contact will be made with Cummins next quarter.

Problems Encountered

None

Publications/Presentations

None

Development of Catalytically Selective Electrodes for NOx and Ammonia Sensors

Timothy Armstrong, Fred Montgomery, and David West
Oak Ridge National Laboratory
P.O. Box 2008, Oak Ridge, TN 37831-6084
Phone: (865) 574-7996, E-mail: armstrongt@ornl.gov

Objective

To develop non-catalytic and catalytically selective electrodes for use in NOx and ammonia sensors and to build and test sensors using the materials and technology developed

Technical Highlights (NOx Sensor Development)

1. ORNL has developed 2 new approaches, that are firsts for NOx sensing:

    a. First, we have developed a sensor that uses only one catalyst for the anodic and cathodic electrode. This design coupled with a current bias, has resulted in a functioning "total NOx" sensor capable of measuring the total NO and NO_2 concentration in a gas stream.

    b. Secondly, using a composite Pt and metal oxide electrode system we have developed a sensor that can measure the NO concentration in an exhaust gas stream.

    c. These 2 sensors coupled together can provide the total NO and NO_2 concentration at any time and temperature.

2. The single material electrode design has demonstrated little or not oxygen sensitivity in early tests.

3. Development and testing of catalysts are still ongoing.

4. A new sensor design was developed this reporting period that allows for the placement of tens to hundreds of sensors in parallel on a single substrate. It is anticipated that this design will improve sensitivity and increase the output single.

Status of Milestones

1. Determine kinetics of NO reaction on electrode as a function of temperature and environment.

    This is ongoing and will continue as new electrode materials are developed and tested as well as new sensor designs.

2. Fabricate and test a prototype NOx sensor (09/03)

   ORNL has fabricated a laboratory prototype sensor capable of measuring 'total" NOx concentrations and will continue this activity to support the ongoing catalyst development.

Problems Encountered

None

Inventions

1. Electrically biased NO_x sensor with co-planar electrodes on a ceramic substrate.

Internal Distribution

B. L. Armstrong, 4515, MS-6063, armstrongbl@ornl.gov
T. R. Armstrong, 4508, MS-6084, armstrongt@ornl.gov
P. F. Becher, 4515, MS-6068, becherpf@ornl.gov
T. M. Besmann, 4515, MS-6063, besmanntm@ornl.gov
C. A. Blue, 4508, MS-6083, blueca@ornl.gov
M. A. Brown, 4500N, MS-6186, brownma@ornl.gov
M. K. Ferber, 4515, MS-6069, ferbermk@ornl.gov
J. A. Haynes, 4515, MS-6063, haynesa@ornl.gov
D. R. Johnson, 4515, MS-6066, johnsondr@ornl.gov
M. A. Karnitz, 4500N, MS-6186, karnitzma@ornl.gov
J. O. Kiggans, 4508, MS-6087, kiggansjojr@ornl.gov
T. J. King, 4515, MS-6065, kingtjjr@ornl.gov
J. W. Klett, 4508, MS-6087, klettjw@ornl.gov
E. Lara-Curzio, 4515, MS-6069, laracurzioe@ornl.gov
H. T. Lin, 4515, MS-6068, linh@ornl.gov
R. A. Lowden, 4515, MS-6063, lowdenra@ornl.gov
P. J. Maziasz, 4500S, MS-6115, maziaszpj@ornl.gov
K. L. More, 4515, MS-6064, morekl1@ornl.gov
R. D. Ott, 4515, MS-6083, ottr@ornl.gov
S. D. Nunn, 4508, MS-6087, nunnsd@ornl.gov
B. A. Pint, 4500S, MS-6156, pintba@ornl.gov
D. T. Rizy, 3147, MS-6070, rizydt@ornl.gov
D. P. Stinton, 4515, MS-6063, stintondp@ornl.gov
R. W. Swindeman, 4500S, MS-6155, swindemanrw@ornl.gov
T. N. Tiegs, 4508, MS-6087, tiegstn@ornl.gov
P. F. Tortorelli, 4500S, MS-6156, tortorellipf@ornl.gov
I. G. Wright, 4500S, MS-6157, wrightig@ornl.gov
A. Zaltash, 3147, MS-6070, zaltasha@ornl.gov

External Distribution

ALLISON ADVANCED DEVELOPMENT CO., 1100 Wilson Blvd., Suite 1450, Arlington, VA 22209
J. Miles, r.jeffrey.miles@allison.com

ALM SYSTEMS, INC, 1920 N Street, NW, Suite 750, Washington, DC 20036
M. Kalin, mkalin@ibek.com

ARGONNE NATIONAL LABORATORY, 9700 S. Cass Ave., Argonne, IL 60439-4838
W. Ellingson, ellingson@anl.gov
J. P. Singh, jpsingh@anl.gov

BATTELLE MEMORIAL INSTITUTE, 505 King Avenue, Columbus, OH 43201
D. Anson, ansond@battelle.org

BAYSIDE MATERIALS TECHNOLOGY, 21150 New Hampshire Ave., Brookville, MD 20833
D. Freitag, dfreitag@ix.netcom.com

BCS, INC., 5550 Sterrett Place, Suite 216, Columbia, MD 21044
D. Bartley, dbartley@bcs-hq.com

BOWMAN POWER, 20501 Ventura Boulevard #285, Woodland Hills, CA 91364
T. Davies, tdavies@bowmanpower.co.uk
T. Hynes, ahynes.bowmanpower@att.net
D. Flaxington, dflaxington@bowmanpower.co.uk

CALIFORNIA ENERGY COMMISSION
A. Soinski, asoinski@energy.state.ca.us

CANNON-MUSKEGON CORP., Box 506, Muskegon, MI 49443-0506
J. Wahl, jwahl@canmkg.com

CAPSTONE TURBINE CORP., 6430 Independence Ave., Woodland Hills, CA 91367
P. Chancellor, pchancellor@capstoneturbine.com
K. Duggan, kduggan@capstoneturbine.com
M. Stewart, mstewart@capstoneturbine.com
J. Willis, jwillis@capstoneturbine.com
M. Rodrigues, mrodrigues@capstoneturbine.com
B. Treece, btreece@capstoneturbine.com

CLEMSON UNIVERSITY, South Carolina Institute for Energy Studies, 386-2, Clemson, SC 29634-5180
L. Golan, glawren@clemson.edu
R. Wenglarz, rwnglrz@clemson.edu
J. Hinson, jhinson@clemson.edu

CONNECTICUT RESERVE TECHNOLOGIES, 2997 Sussex Ct., Stow, OH 44224
E. Baker, baker@crtechnologies.com
S. Duffy, sduffy@crtechnologies.com
J. Palko, jpalko@crtechnologies.com

DTE ENERGY, 37849 Interchange Dr., Suite 100, Farmington Hills, MI 48335
M. Davis, davism@dteenergy.com

ELECTRIC POWER RESEARCH INSTITUTE, 3412 Hillview Ave., Palo Alto, CA 94303
J. Stringer, jstringe@epri.com

ELGILOY SPECIALTY METALS, 1565 Fleetwood Drive, Elgin, IL 60123
T. Bartel, terryb@elgiloy.com

ELLIOTT ENERGY SYSTEMS, 2901 S.E. Monroe Street, Stuart, FL 34997
D. Burnham, dburnham@elliott-turbo.com
D. Dewis, ddewis@elliott-turbo.com

ENERGETICS, INC., 501 School St., SW, Suite 500, Washington, DC 20024
R. Scheer, rscheer@energeticsinc.com

ENERGY TECHNOLOGIES APPLICATIONS, 5064 Camino Vista Lujo, San Diego, CA 92130-2849
T. Bornemisza, borneger@ix.netcom.com

GAS TURBINE ASSOCIATION, 1050 Thomas Jefferson St., NW, 5th Fl, Washington, DC 20007
J. Abboud, abboud@advocatesinc.com

GENERAL ELECTRIC (GE) CR&D, 1 Research Circle, Building K1-RM 3B4, Niskayuna, NY 12309
S. Correa, correa@crd.ge.com
K. Luthra, luthra@crd.ge.com
M. VanDerwerken, vanderwerken@crd.ge.com
C. Johnson, johnsonca@crd.ge.com

GENERAL ELECTRIC AIRCRAFT ENGINES, One Neumann Way, Mail Drop M89, Cincinnati, OH 45215-1988
R. Darolia, ram.darolia@ae.ge.com

GENERAL ELECTRIC POWER SYSTEMS, One River Rd., 55-127, Schenectady, NY 12345
R. Orenstein, robert.orenstein@ps.ge.com

GENERAL ELECTRIC POWER SYSTEMS, Gas Technology Center, 300 Garlington Road, Greenville, SC 29615
P. Monaghan, philip.monagham@ps.ge.com

HAYNES INTERNATIONAL, INC., 1020 W. Park Avenue, P.O. Box 9013, Kokomo, IN 46904-9013
V. Ishwar, vishwar@haynesintl.com
D. Klarstrom, dklarstrom@haynesintl.com

HONEYWELL CERAMIC COMPONENTS, 2525 W. 190th St., Torrance, CA 90504
D. Foley, dan.foley@honeywell.com
C. Li, chien-wei.li@honeywell.com
D. Newson, danielle.newson@honeywell.com
M. Savitz, MaxineSavitz@aol.com
J. Wimmer, jim.wimmer@honeywell.com
M. Mitchell, michele.mitchell@honeywell.com

HONEYWELL COMPOSITES, 1300 Marrows Rd., PO Box 9559, Newark, DE 19714-9559
L. Connelly, liz.connolly@ps.ge.com
P. Gray, paul1.gray@ps.ge.com
D. Landini, dennis.landini@ps.ge.com

HONEYWELL ENGINES, SYSTEMS, & SERVICES 2739 E. Washington St., PO Box 5227, Phoenix, AZ 85010

B. Schenk, bjoern.schenk@honeywell.com

HONEYWELL POWER SYSTEMS, 8725 Pan American Freeway NE, Albuquerque, NM 87113

S. Wright, e.scott.wright@honeywell.com

HOWMET RESEARCH CORP., 1500 South Warner St., Operhall Research Center, Whitehall, MI 49461-1895

B. Mueller, bmueller@howmet.com

R. Thompson, rthompson@howmet.com

INGERSOLL-RAND ENERGY SYSTEMS, 32 Exeter St., Portsmouth, NH 03801

A. Kaplau-Colan, alex_haplau-colan@ingersoll-rand.com

M. Krieger, michael_krieger@irco.com

J. Johnson, jay_johnson@ingersoll-rand.com

J. Kesseli, jim_kesseli@ingersoll-rand.com

J. Nash, jim_nash@ingersoll-rand.com

KENNAMETAL INC. 1600 Technology Way, P.O. Box 231, Latrobe, PA 15650-0231

R. Yeckley, Russ.yeckley@kennametal.com

KINECTRICS NORTH AMERICA, 124 Balch Springs Circle, SW, Leesburg, VA 20175

B. Morrison, blake.Morrison@kinectrics.com

KRUPP VDM TECHNOLOGIES CORP., 11210 Steeplecrest, Suite #120, Houston, TX 77065-4939

D. Agarwal, dcagarwal@pdq.net

NASA GLENN RESEARCH CENTER, 21000 Brookpark Rd., MS 49-7, Cleveland, OH 44135

D. Brewer, david.n.brewer@grc.nasa.gov

J. Gykenyesi, john.p.gyekenyesi@lerc.nasa.gov

S. Levine, stanley.r.levine@lerc.nasa.gov

N. Nemeth, noel.n.nemeth@grc.nasa.gov

B. Opila, opila@grc.nasa.gov

NATIONAL RURAL ELECTRIC COOPERATIVE ASSOC., 4301 Wilson Blvd., SS9-204, Arlington, VA 22203-1860

E. Torrero, ed.torrero@nreca.org

NATURAL RESOURCES CANADA, 1 Haanel Drive, Nepean, Ontario, Canada K1A 1M1

R. Brandon, rbrandon@nrcan.gc.ca

PCC AIRFOILS, INC., 25201 Chagrin Blvd., Suite 290, Beachwood, OH 44122

C. Kortovich, ckortovich@pccairfoils.com

PENN STATE UNIVERSITY, Applied Research Laboratory, PO Box 30, State College, PA 16823
J. Singh, jxs46@psu.edu

RICHERSON AND ASSOC., 2093 E. Delmont Dr., Salt Lake City, UT 84117
D. Richerson, richersond@aol.com

ROLLS-ROYCE ALLISON, 2925 W. Minnesota St., PO Box 420, Indianapolis, IN 46241
S. Berenyi, steve.g.berenyi@allison.com
P. Heitman, peter.w.heitman@allison.com
F. Macri, francis.g.macri@allison.com
J. Oswald, jim.oswald@rolls-royce.com

SAINT-GOBAIN CERAMICS & PLASTICS, INC., Goddard Road, Northboro, MA 01532
B. LaCourse, Brian.C.LaCourse@saint-gobain.com
R. Licht, robert.h.licht@saint-gobain.com
M. Abouaf, Marc.Abouaf@saint-gobain.com
V. Pujari, Vimal.K.Pujari@saint-gobain.com
A. Vartabedian, Ara.M.Vartabedian@saint-gobain.com

SEBESTYEN, T., Consultant, 6550 Mission Ridge, Traverse City, MI 49686-6123
T. Sebestyen, sebestyen@chartermi.net

SIEMENS WESTINGHOUSE POWER CORP., 1310 Beulah Rd., Pittsburgh, PA 15235-5098
M. Burke, michael.burke@swpc.siemens.com
C. Forbes, christian.forbes@swpc.siemens.com

SOLAR TURBINES, INC., TurboFab Facility, 16504 DeZavala Rd., Channelview, TX 77530
B. Harkins, harkins_bruce_d@solarturbines.com

SOLAR TURBINES INC., 818 Connecticut Ave., NW, Suite 600, Washington, DC 20006-2702
R. Brent, solardc@bellatlantic.net

SOLAR TURBINES, INC., 2200 Pacific Highway, PO Box 85376, MZ R, San Diego, CA 92186-5376
P. Browning, browning_paul_f@solarturbines.com
M. Fitzpatrick, fitzpatrick_mike_d@solarturbines.com
P. Montague, montague_preston_j@solarturbines.com
M Van Roode, van_roode_mark_x@solarturbines.com
M. Ward, ward_mike_e@solarturbines.com
J. Price, jeffprice@solarturbines.com

SOUTHERN CALIFORNIA EDISON COMPANY, 2244 Walnut Grove Avenue, Rosemead, CA 91770
S. Hamilton, hamiltsl@sce.com

SOUTHERN COMPANY, 600 N. 18th Street, 14N-8195, P.O. Box 2641, Birmingham, AL 35291
S. Wilson

STEVEN I. FREEDMAN, Engineering Consultant, 410 Carlisle Ave., Deerfield, IL 60015
S. Freedman, sifreedman@aol.com

STAMBLER ASSOCIATES, 205 South Beverly Drive, Suite 208, Beverly Hills, California 90212
I. Stambler

THE BOEING COMPANY, Rocketdyne Propulsion & Power, 6633 Canoga Avenue
MC: GB-19, P.O. Box 7922, Canoga Park, CA 91309-7922
G. Pelletier, gerard.pelletier@west.boeing.com

TELEDYNE CONTINENTAL MOTORS, 1330 W. Laskey Rd., PO Box 6971, Toledo, OH 43612-0971
J. T. Exley, texley@teledyne.com

TURBEC
L. Malmrup, lars.malmrup@turbec.com

UCI COMBUSTION LABORATORY, U. of CA, Irvine, Irvine, CA 92697-3550
V. McDonell, mcdonell@ucic1.uci.edu

UDRI, Ceramic & Glass Laboratories, 300 College Park Ave., Dayton, OH 45469-0172

A. Crasto, allan.crasto@udri.udayton.edu
G. Graves, gravesga@udri.udayton.edu
N. Osborne, osborne@udri.udayton.edu
R. Wills, roger.wills@udri.udayton.edu

UNITED TECHNOLOGIES RESEARCH CENTER, 411 Silver Lane MS 129-24, East Hartford, CT 06108
H. Eaton, eatonhe@utrc.utc.com
J. Holowczak, holowcje@utrc.utc.com
T. Rosfjord, rosfjotj@utrc.utc.com
J. Smeggil, smeggijg@utrc.utc.com
G. Linsey, linseygd@utrc.utc.com
J. Shi, shij@utrc.utc.com
E. Sun, suney@utrc.utc.com
D. Mosher, mosherda@utrc.utc.com

UNIVERSITY OF CALIFORNIA, Department of Mechanical Engineering, Berkeley, CA 94720
R. Dibble, rdibble@newton.berkeley.edu

UNIVERSITY OF MARYLAND, Department of Mechanical Engineering, College Park, MD 20742-3035
R. Radermacher, rader@eng.umd.edu

UNIVERSITY OF WESTERN ONTARIO, Faculty of Engineering, London, Ontario, Canada N6G 4K1
B. E. Thompson, Thompson@eng.uwo.ca
A. G. Straatman, astraat@engga.uwo.ca

US DOE-NETL, P. O. Box 880, MSO-D01, 3610 Collins Ferry Rd., Morgantown, WV 26507-0880
C. Alsup, Jr., charles.alsup@netl.doe.gov
A. Layne, abbie.layne@netl.doe.gov
L. Wilson, lane.wilson@netl.doe.gov

US DOE-NETL, PO Box 10940, Pittsburgh, PA 15236
N. Holcombe, norman.holcombe@netl.doe.gov
U. Rao, rao@netl.doe.gov

US DOE CHICAGO OPERATIONS OFFICE, 9800 S. Cass Ave., Argonne, IL 60439
J. Jonkouski, jill.jonkouski@ch.doe.gov
J. Mavec, joseph.mavec@ch.doe.gov
J. Livengood, joanna.livengood@ch.doe.gov
S. Waslo, stephen.waslo@ch.doe.gov

US DOE-HQ, 1000 Independence Ave., S.W., Washington DC 20585
R. Fiskum, ronald.fiskum@ee.doe.gov
D. Haught, debbie.haught@ee.doe.gov
P. Hoffman, patricia.hoffman@ee.doe.gov
W. Parks, william.parks@ee.doe.gov
M. Smith, merrill.smith@ee.doe.gov
C. Sorrell, charles.sorrell@ee.doe.gov

WILLIAMS INTERNATIONAL, 2280 West Maple Rd., PO Box 200, Walled Lake, MI 48390-0200
G. Cruzen, g.cruzen@williams-int.com
W. Fohey, w.fohey@williams-int.com
C. Schiller, cschiller@williams-int.com

WRIGHT PATTERSON AIRFORCE BASE,
R. Sikorski, ruth.sikorski@wpafb.af.mil